Alternative Shapes for HYPERION; an Aerodynamically Controlled Re-entry Vehicle

Zandbergen, B.T.C.; Veldman, S

Publication date
1997

Document Version
Final published version

Citation (APA)
Zandbergen, B. T. C., & Veldman, S. (1997). *Alternative Shapes for HYPERION; an Aerodynamically Controlled Re-entry Vehicle*. Delft University of Technology.

Alternative Shapes for HYPERION; an Aerodynamically Controlled Re-entry Vehicle

May 1997

S.M. Veldman and B.T.C. Zandbergen

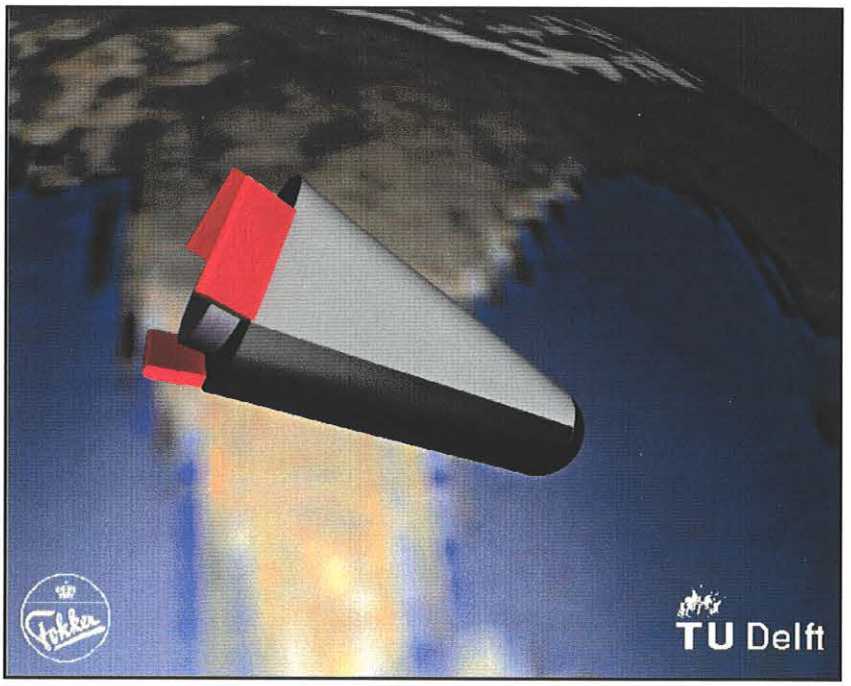

TU Delft
Delft University of Technology

Faculty of Aerospace Engineering

Alternative Shapes for HYPERION; an Aerodynamically Controlled Re-entry Vehicle

S.M. Veldman[1] and B.T.C. Zandbergen[1]
[1] Delft University of Technology, Faculty of Aerospace Engineering
Fax: +31 15 278 5322 email: B.T.C.Zandbergen@lr.tudelft.nl

Abstract

This paper investigates the aerodynamic and stability characteristics of the aerodynamically controlled re-entry test vehicle HYPERION and two alternative vehicles. The baseline vehicle is a moderate lift-to-drag ratio (*L/D*) re-entry capsule with a triangular cross-section and a blunt nose, and has originally been designed by Fokker Space (FS) and the Faculty of Aerospace Engineering of Delft University of Technology (DUT-FAE). The two alternatives are a capsule with a square cross-section and a blunt nose, and a blunted sliced cone.

Vehicle dimensions are optimized for maximum lift-to-drag ratio (*L/D*), using a sequential quadratic programming algorithm. Maximum *L/D* yields maximum cross- and down-range, gives more flexibility regarding the choice of landing site and takes care of uncertainties in aerodynamic characteristics, entry conditions as well as the atmospheric conditions on the predictability of the landing site.

Subsequently, the vehicles are compared on basis of longitudinal stability in the hypersonic flight regime ($M > 5$). Stability characteristics that allow a generous travel of the centre of mass (*c.o.m.*) are favoured because they give flexibility in location of the *c.o.m.* and reduce the influence of uncertainties in vehicle aerodynamics and *c.o.m.* location on a stable and controllable re-entry.

The original method that has been used to design HYPERION is refined to allow calculation of the aerodynamics using the exact geometry. This is needed to distinguish between the quite similar shapes of the alternatives. Furthermore, a selection is made for a convective heat flux method, by comparing several methods available from literature. Finally, the heat flux constraint, based on the Chapman heat flux, has been replaced by a wall temperature constraint using an equilibrium wall temperature and the convective heat flux method of Tauber. Wall temperature has the advantage that it relates directly to the thermal protection system (TPS) materials.

Compared to the earlier design the lift-to-drag ratio has increased by 20 %, because of the refined method that uses the exact geometry and because of reduction of the vehicle mass. The new heat flux method, however, puts a more stringent constraint. The final result is that the three vehicles do not differ much in *L/D*, but the sliced blunted cone offers a considerably larger *c.o.m.* travel.

Nomenclature

C	[varies]	constant in equation (4)
c_f	[m]	flap chord
C_D	[-]	drag coefficient
C_L	[-]	lift coefficient
C_M	[-]	moment coefficient
C_{M_α}	[deg^{-1}]	$\frac{\partial C_M}{\partial \alpha}$
g	[m/s^2]	gravitational acceleration
h	[m]	altitude
H	[J]	enthalpy
L	[m]	length
m	[kg]	mass
M	[-]	Mach number
M	[-]	power in equation (4)
N	[-]	power in equation (4)
L/D	[-]	lift-to-drag ratio
$\dot{q}$	[W/m^2]	heat flux
R	[m]	radius
R_0	[m]	earth's radius
S_{ref}	[m^2]	reference area
T	[K]	temperature
V	[m/s]	velocity
V	[m^3]	volume
α	[°]	angle of attack
γ	[°]	flight path angle
δ	[°]	flap deflection angle
ε	[-]	emissivity
η	[-]	efficiency
θ	[°]	cone angle
ρ	[kg/m^3]	density
σ	[°]	slice angle
σ	[W/(m^{2}K^4)]	Stefan-Boltzmann constant

Subscripts

AW	adiabatic wall
B	base
Body	body
c	circular
conv	convective
des	design
f	flap
N	nose
rad	radiative
S	slice
vol	volume
W	wall

Acronyms

ARD	Ariane Re-entry Demonstrator
c.o.m.	centre of mass
DUT	Delft University of Technology
FAE	Faculty of Aerospace Engineering

FS	Fokker Space
HYFLEX	HYpersonic FLight EXperiment
HYPERION	HYPErsonic Re-entry Investigation Of the Netherlands
PEACH	Program for Estimation of Aerodynamic Characteristics of Hypersonic vehicles
TPS	Thermal Protection System

1 Introduction

This paper presents an exploratory study into possible concepts for an aerodynamically controlled re-entry test vehicle which is supposed to be used for the qualification of new technologies and theoretical models in the fields of thermal protection systems (TPS), navigation systems, guidance and control systems, as well as hypersonic aerothermodynamics for advanced launchers.

The qualification will be particularly valuable in those flight ranges of typical advanced launchers which cannot be simulated by ground-based facilities, and where results of computational fluid dynamics need validation data [Sudmeijer *et al.*, 1989; Mooij *et al.*, 1995]. Thus, the main task of the vehicle will be to make an aerodynamically controlled flight in these ranges.

Furthermore, the vehicle is to have optimal aerodynamic characteristics. A high lift-to-drag ratio is preferable for flexibility in landing site (maximum cross and down range), it allows for control studies, and it takes care of uncertainties in injection and atmospheric conditions [Harris, 1980]. Good trim and static stability characteristics allow a large travel of the centre of mass (*c.o.m.*), which gives flexibility for changing *c.o.m.* due to for instance use of thrusters, and also take care of uncertainties in aerodynamics and estimation of *c.o.m.* location. This study only considers the longitudinal characteristics. No quantitative requirement is set for these characteristics, but they are treated as the larger the better.

The vehicle will be launched by Ariane V, but should also allow launch by a sounding rocket.

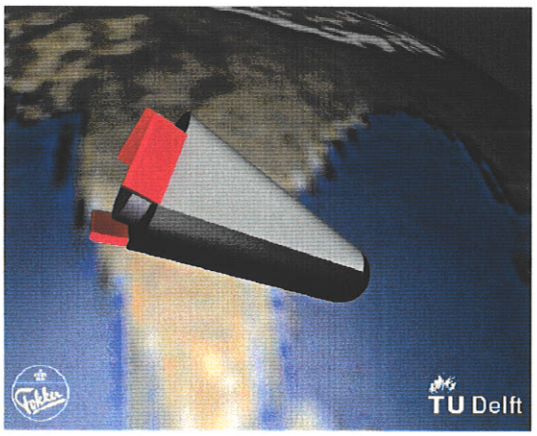

Figure 1: HYPERION [Mooij *et al.*,1995]

An earlier study at DUT-FAE [Mooij *et al.*, 1995] investigated a triangular shaped vehicle called HYPERION (see figure 1). The triangular cross-section was chosen to locate three control flaps at its base to control pitch, yaw and roll. The configuration was optimized for maximum lift-to-drag ratio, at a constant density provided for by F.S. which was supposed to be a good mean for re-entry vehicles.

New information from Fokker Space about launch possibilities indicated that the mass of the vehicle was much too high, and that it should be redesigned for a lower mass. Also a study by [Romagnoli, 1996] indicated that heat flux constraints should be lowered considerably, which also would need a vehicle with a lower mass. Furthermore, stability and control characteristics of HYPERION showed large sensitivity to location of the centre of mass.

This paper takes a more general stand, by not only focusing on HYPERION, but also two other shapes, to see how HYPERION compares to these shapes on basis of aerodynamic quality and longitudinal attitude control and static stability in the hypersonic flight regime ($M > 5$). Furthermore, in this study refinements have been made to the design process of Mooij *et al.*. This includes the use of the exact geometry for aerodynamic calculations, the use of wall temperature as constraint instead of heat flux, and the use of a different convective heat flux method.

Figure 2 shows the design schematic. In a first step the different concepts (shapes) are optimized for a maximum, untrimmed lift-to-drag ratio. For each concept an optimum configuration is selected that has the required mass with optimum aerodynamics, using an optimum trajectory with constraints on the wall temperature, dimensions and density. A second step studies the stability of the vehicles, and determines the allowable travel of the centres of mass and the sensitivity to flap chord lengths.

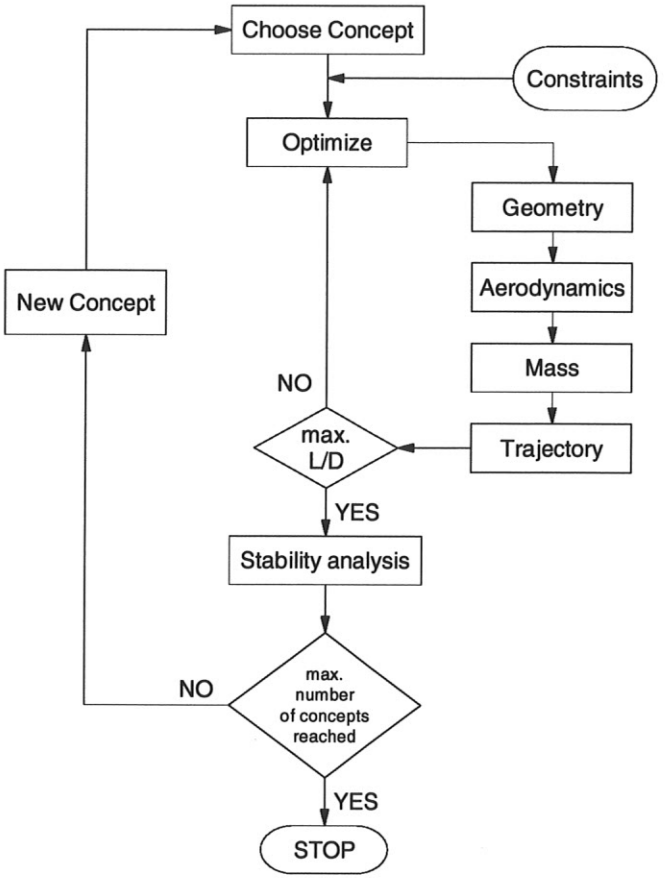

Figure 2: Design schematic

For a proper selection of a shape of the re-entry vehicle further attention is required for at least directional stability, in particular at high angles of attack, stability at supersonic and subsonic speeds (in particular shift of the centre of pressure), weight estimation and TPS design, flow phenomena, and structural layout. These subjects should be addressed in a follow-on study.

The first section of this paper presents a more detailed description of the requirements and constraints of the re-entry vehicles.
The second section presents the baseline concept together with two other concepts. Section 3 discusses the methods used, and section 4 checks the methods. Section 5 presents the results for the 3 vehicles and gives a final selection. Section 6 states conclusions and recommendations.

2 Requirements and constraints

The overall requirement for the vehicle is that it should obtain maximum lift-to-drag ratio in order to obtain a maximum cross range, low acceleration loads and low heat fluxes [Vinh,1980], for a mass of 250 kg.

Other general requirements can be defined when considering the volumetric efficiency, and the mean density of known re-entry vehicles.

Figure 3 shows the volumetric efficiency, η_{vol}, as function of the lift-to-drag ratio, with the volumetric efficiency being the ratio between volume and surface area. For a high *L/D* it is clear that the volumetric efficiency decreases due to "flattening" the body and/or applying wings, strakes and other lifting surfaces. However, applying these surfaces increases complexity and cost of the vehicle. Therefore we limit this study to bodies only, and apply control surfaces directly to the body.

Table 1 shows the overall mass and mean density for a number of ballistic (C_L = 0), semi-ballistic (*L/D* = 0.3-0.8) and lifting or gliding re-entry (*L/D* > 0.8). The lifting vehicle HYFLEX has a density of about 300 kg/m^3. The semi-ballistic Colibri (*L/D* = 0.6) and the Ariane Re-entry Demonstrator (ARD) (*L/D* = 0.3) have a considerable range in density of 250 kg/^{3} to 440 kg/m^3. The remaining vehicles are ballistic, and have densities in excess of 440 kg/m^3. These values do not indicate a straight trend at first sight. Therefore vehicle densities of 200 to 500 kg/m^3 are allowed.

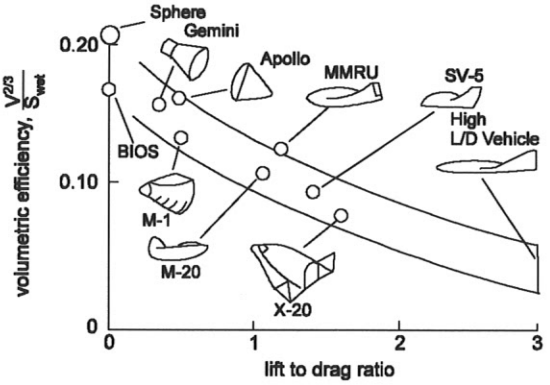

Figure 3: Volumetric efficiency of several re-entry vehicles as function of lift-to-drag ratio [Stewart *et al*, 1969]

	Mass [kg]	Density [kg/m^3]
Discoverer [Jane's,1964]	136	560
Carina [MPSO,1995]	160	466
Colibri [Schöttle,1995]	170	250
HYFLEX [Shirouzu,1993]	1048	308
Mercury [Jane's,1969]	1130	440
ARD [Cazaux,1995]	2800	438

Table 1: Masses and mean densities of several re-entry vehicles

The re-entry conditions will be typical LEO re-entry conditions, and they are assumed to be equilibrium glide conditions, which means that the flight path angle is small, and that the absolute velocity is near the circular speed. The wall temperature is considered to be the only flight path constraint. We assume a reinforced carbon carbon composite

nose cap, which has a maximum allowable temperature of 2089 K for single use. Other flight path constraints, such as maximum acceleration and maximum dynamic pressure, are ignored, because they are of minor importance for vehicles making a lifting re-entry.

The vehicle dimensions, based on data of Fokker Space, are such that it could fit in the Ariane 5 interstage: length does not exceed 1.9 m and base diameter is 0.5 m.

During re-entry the vehicle should be trimmable and statically stable between 15° and 45° angle of attack. Figure 4 shows a typical angle of attack modulation during re-entry. The high angle of attack (± 45°) during the first phase of re-entry keeps maximum heat flux and wall temperature down, because at α = 45° the maximum lift coefficient occurs. Subsequently the angle of attack is lowered to 15° to 20°, where the maximum lift-to-drag ratio is located, to obtain maximum cross range. For trim, flap deflections of -5° to 15° are allowed, which is analogous to the study of [Sudmeijer, 1996]. The flap deflection δ (see figure 5) is defined as the angle between the x-axis and the flap, and is positive for outward deflections.

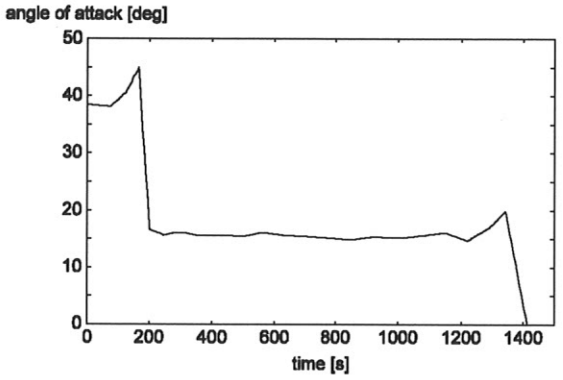

Figure 4: Typical angle of attack modulation for a re-entry trajectory for maximum range [Teutsch *et al.*, 1997]

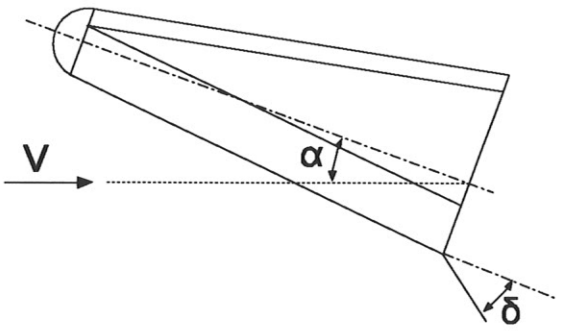

Figure 5: Definition of the angle of attack α and the flap deflection angle δ

3 Concepts

Figure 6 shows the baseline concept HYPERION taken from [Mooij *et al.*, 1994]. The vehicle has a nose radius (R_N) of 0.24 m, a semi-cone angle (θ) of 9° and a mass of 547 kg. Besides its large mass, the

vehicle has a number of other drawbacks, in particular sensitivity for change in centre of mass in x-direction, strong coupling of roll and yaw, and flow separation at the flanks when flying at high angle-of-attack [Huizinga, 1996], which affects the flaps located at these flanks.

Figures 8 and 9 show the other concepts considered: a Delta-Clipper-like shape, with a square cross-section and a sliced blunted cone (after this called Delta). The sliced cone can be compared to the Colibri vehicle [Schöttle, 1994], and it is investigated because of its better stability characteristics. To accommodate the bank-to-turn mode for the sliced cone, the flap should be split. Furthermore Delta should have better flow condition at the flanks, and facilitate the uncoupling of roll and yaw.

The geometry of both HYPERION and Delta are fully defined using the cone angle θ, and the nose and base radii, R_N and R_B. For the sliced cone two additional parameters are needed, i.e. the length of the slice L_S and the angle of the slice σ. An important dependent vehicle dimension is the flap width L_f, which is taken equal to the width of the flat underside. The flap chord c_f is taken 0.2 m, equal to the value used in the study of [Mooij *et al.*, 1995], for all three vehicles. Only the lower flap (for HYPERION and Delta) will be considered.

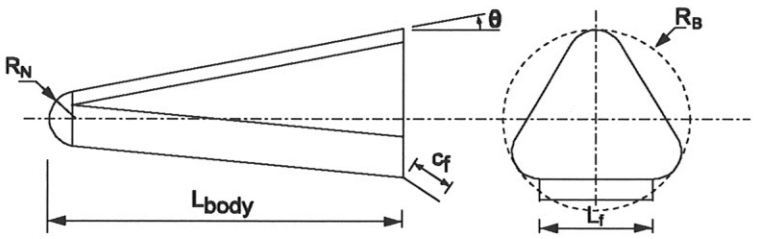

Figure 6: Configuration of HYPERION

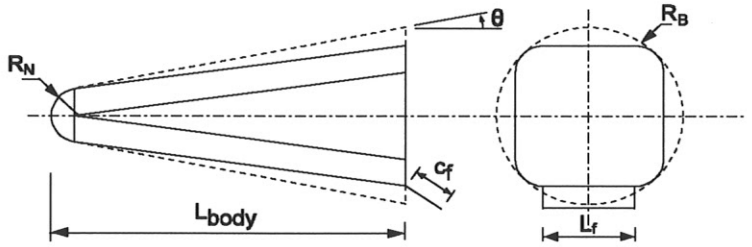

Figure 7: Configuration of Delta

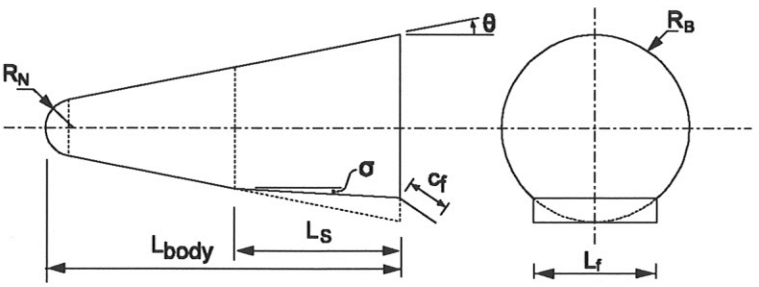

Figure 8: Configuration of a sliced cone

Table 2 gives the independent geometry variables for each vehicle. For all vehicles the base radius is set at 0.5 m as in previous studies. An additional independent variable is the angle of attack for which the maximum *L/D* is obtained, called the design angle of attack, α_{des}.

Hyperion	Delta	Sliced Cone
θ	θ	θ
R_N	R_N	R_N
		σ
		L_S

Table 2: Independent geometry variables

4 Design Methods

4.1 Aerodynamics

The earlier study of [Mooij *et al.*, 1995] has used a blunted cone approximation of HYPERION to estimate aerodynamics. If we would do this for all three vehicle shapes, it is clear that not too many differences between them will come to light. Therefore a hypersonic aerodynamics program PEACH of [Veldman, 1994] has been used, which uses the same theoretical models as the blunted cone approximation, but which allows an exact description of the geometry. Accuracy of the program is about 15%. The use of PEACH resulted, as shown in table 3, in a considerable increase in lift-to-drag ratio, and decrease of the nose radius. Figure 9 shows the pressure distribution on HYPERION determined using Modified Newtonian on the windward side, Prandtl-Meyer expansion from free stream at the leeward side, and Newtonian at the base (i.e. $C_p = 0$).

	blunted cone approximation	exact geometry PEACH
L/D_{max} [-]	1.16	1.49
cone angle [°]	10.89	11.64
nose radius [m]	0.163	0.133

Table 3: Comparison of results between blunted cone approximation and exact geometry, mass = 250 kg, maximum heat flux = 1.6 MW/m^2

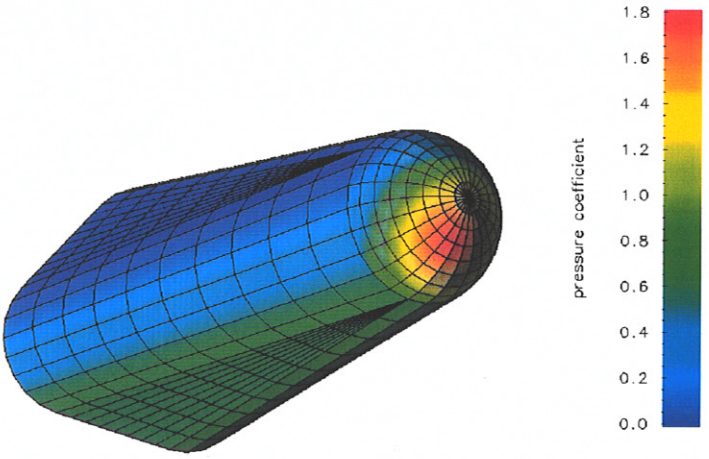

Figure 9: Pressure distribution on HYPERION

4.2 Trajectory

For the atmospheric entry the equilibrium glide trajectory is assumed. The equilibrium glide path is flown by vehicles, such as the Space Shuttle, that have adequate lift, since the path affords low deceleration loads and low heat fluxes [Tauber,1986]

Following Tauber we find the flight path expression for the equilibrium glide path:

$$L - mg = -\frac{m V^2}{R_0} \tag{1}$$

Where L is the lift, m is the mass, g is the gravitational acceleration, V is the velocity and R_0 is the earth radius. This equation gives:

$$\frac{\rho V^2}{V_c^2 - V^2} = \frac{2}{R_0} \frac{m}{C_L S_{ref}} \tag{2}$$

where ρ is the density and V_c is the circular satellite speed. The right hand side can be considered constant during the high speed portion of the entry.

The flight path expression, equation (2), is given in its simplest form, which neglects the earth's rotation and also assumes the changes in g and R_0 to be negligible.

4.3 Wall temperature

During conceptual design the wall temperature and the heat flux can be estimated using the equilibrium condition between radiative and convective heat flux. Equilibrium can be assumed for thin shelled construction, such as the C/C nose cap, which has a small heat capacity and limited conduction and radiation to the surrounding structure [Veldman *et al.*,1997].

The radiative heat flux is expressed by:

$$\dot{q}_{rad} = \varepsilon \sigma T_w^4 \tag{3}$$

and the convective heat flux has the form of:

$$\dot{q}_{conv} = C \rho^M V^N \left(1 - \frac{H_W}{H_{AW}}\right) \tag{4}$$

where C, M and N are assumed to be constant. Different values can be assumed, which are presented in table 4.

	C [varies]	M [-]	N [-]	Remarks
[Chapman[1)],1959]	$1.93\ 10^{-4}$	0.5	3	$H_W/H_{AW} = 0$
[Kemp and Ridell,1957]	$2.53\ 10^{-5}$	0.5	3.25	Theoretical model
[Tauber et al, 1986]	$1.83\ 10^{-4}$	0.5	3	fit on flight data

Table 4: Constants for convective heat flux methods

In case of the methods of Kemp and Tauber, the heat flux is a weak function of the wall enthalpy. Tauber and Kemp show that for adequate results a calorically perfect gas ($\Delta h = c_p \Delta T$) can be assumed. To obtain the equilibrium values for heat flux and wall temperature it is needed to iterate between equations. (3) and (4), or use a direct solution [Veldman *et al.*, 1997].

To check which method is best used, the equilibrium heat fluxes and wall temperatures are calculated along an equilibrium glide trajectory of equation (2) for typical characteristics of the STS-5 mission [Curry, 1986; Williams, 1984].

The peak values for maximum heat flux and wall temperature for this mission were 450 kW/m^2 and 1644 K respectively. Note that with a simple check using equation (3) and an emissivity of 0.8 we learn that these two values are not an equilibrium for radiative and convective heat flux. This can be explained by conduction to the surrounding structure and by radiation from the inside of the nose cone which decrease the wall temperature.

Figures 10 and 11 show the different methods as compared to the Shuttle data. Note that the heat fluxes differ considerably up to a factor two. Because of the nature of the radiative heat flux equation, the resulting wall temperatures show a more limited difference.

Tauber overestimates both heat flux and temperature but gives the best results. Most important is the effect of the different methods on the final results (i.e. the maximum L/D). Using the method of Kemp and Ridell, as compared to Tauber's method, yields a decrease of L/D_{max} of about 25%.

The method of Tauber is selected, because it has been derived using flight data.

Maximum wall temperature is assumed to occur during maximum heating. Convective heating is still a function of wall temperature, but

at maximum heating we can assume T_W/T_{AW} to be 0.1 according to [Koppenwallner, 1988]. The expression for peak heating rate in vehicle parameters only is now (with m and S_{ref} are the mass and reference area respectively):

$$\dot{q}_{max} \propto \left(\frac{m}{R_N C_L S_{ref}} \right)^M \tag{5}$$

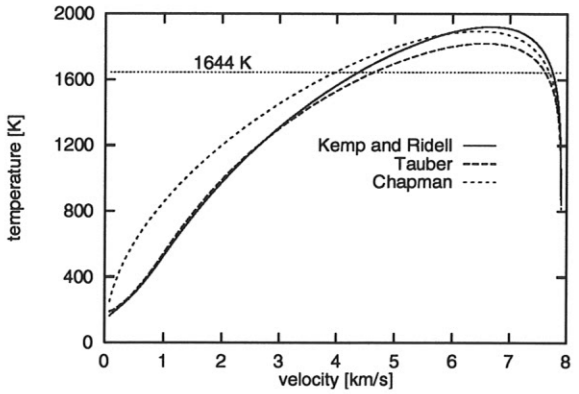

Figure 10: Equilibrium temperature along an equilibrium flight trajectory, for a vehicle having Space Shuttle characteristics

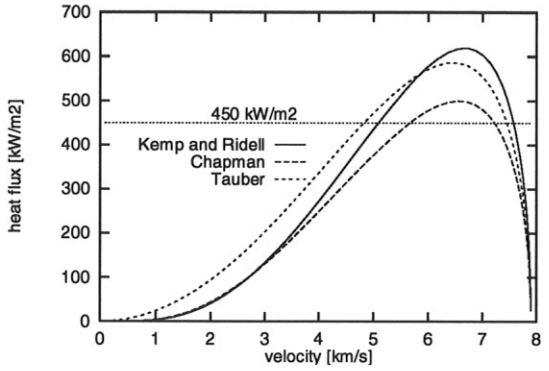

Figure 11: Equilibrium heat flux along an equilibrium flight trajectory, for a vehicle having Space Shuttle characteristics

4.3 Optimization

Optimization is performed using a successive quadratic programming method, coded in a subroutine taken from the IMSL library [IMSL, 1987]. In contrast to the MATLAB routine used in previous studies it allowed the inclusion of PEACH into the optimization loop. This means that the angle of attack has become an independent variable in the optimization process, along with the nose radius and cone angle. the vehicle should fly at this angle of attack to obtain maximum cross and down range.

Furthermore, using PEACH does away with the need for parametrically splined aerodynamic data, as was used in the MATLAB routine. It also facilitates the use of vehicles that are characterized by more than 3 independent variables, because making a spline of more than 3 parameters would be improbable.

Putting PEACH directly in the optimization loop resulted in a further increase of the lift-to-drag ratio as shown in table 5. This difference is

due (1) to the uncertainties in the spline approximation of the aerodynamics and (2) that the angle of attack has become a variable in the optimization process.

	spline approximation	aerodynamics in the loop
L/D_{max} [-]	1.49	1.63
cone angle [°]	11.64	12.34
nose radius [m]	0.133	0.105

Table 5: Comparison between spline approximation and aerodynamics in the loop

4.4 Trim and static stability

Trim ($C_M = 0$) and static stability ($C_{M_\alpha} < 0$) are accomplished by suitable location of the centre of mass and by flap deflection. Lines of $C_M = 0$, and areas of $C_{M_\alpha} < 0$ for the possible angles of attack and flap deflection angles delimit an area where the centre of mass has to be located. The static derivative C_{M_α} is approximated by taking the finite difference between the values of C_M at a certain angle of attack and at the same angle increased by half a degree:

$$C_{M_\alpha} = \frac{C_M(\alpha + 0.5°) - C_M(\alpha)}{0.5} \qquad (6)$$

The flap is assumed to be a flat plate. At the back side (i.e. the side facing the base) base pressure is applied, and at the side facing the flow, the regular pressure methods are used.

5 Results

The results give (1) a comparison between the baseline and the newly designed HYPERION, (2) a comparison between the three vehicles for their *L/D* and vehicle dimensions, (3) the *c.o.m.* travel allowed and (4) the sensitivity to flap chord length.

Table 6 shows the lift-to-drag ratio and dimension for the baseline method, and the refined method. In comparing the results we should consider that the baseline was optimized for a constant density of 800 kg/m^3 and a maximum heat flux of 2 MW/m^2, on the other hand the update was optimized for a constant mass of 250 kg and a maximum wall temperature of 2089 K.

The update has a considerably higher *L/D* than the baseline, this is in particular because the nose radius is smaller, which has two effects that increase *L/D*. First it makes the nose less blunt and therefore decreases C_D. Secondly a smaller nose radius results in a larger flat underside, which increases C_L. The smaller nose radius is possible because the mass is much smaller, as illustrated by equation (5). A third positive effect is the use of the exact geometry as illustrated

by table 3. The only effect that holds a further increase of *L/D* is the wall temperature constraint of 2089 K, which is much more constraining then a heat flux of 2 MW/m^2. The temperature constraint of 2089 K can be compared to a heat flux constraint of about 900 kW/m^2.

	Baseline	Update
L/D [-]	0.89	1.07
θ [°]	9	10
R_N [m]	0.24	0.195
mass [kg]	547	250

Table 6: Comparison between baseline and update of HYPERION

Table 7 shows the lift-to-drag ratio, vehicle dimensions, and the angle of attack for maximum lift-to-drag ratio. Lift-to-drag ratio's for all three vehicles are in the same order of magnitude. All vehicles have the maximum length of 1.9 m, which is profitable, because length is proportional to lift, i.e. the longer the vehicle, the larger C_L and *L/D*, and the lower the wall temperature. The same holds for the slice length of sliced cone, which tends to take the complete length of the vehicle, more or less changing it to a flat plate.

Probably the most significant difference between the vehicles is the width of the flap. Delta can only have a flap width of 0.42 m, whereas the sliced cone has almost twice that width, and has therefore a restoring moment twice as high.

	HYPERION	Delta	Sliced Cone
L/D [-]	1.07	1.01	0.98
θ [°]	10.1	9.7	9.7
R_N [m]	0.195	0.207	0.208
σ [°]	-	-	0.0
L_S [m]	-	-	1.0 *
α_{des} [°]	27	26	28
L_{body} [m]	1.9 *	1.9 *	1.9 *
η_{vol} [-]	0.156	0.160	0.155
ρ [kg/m^3]	454	394	477
L_f [m]	0.53	0.42	0.75

* upper boundary reached

Table 7: Results for optimization to maximum lift-to-drag ratio of untrimmed vehicles

Figure 12 shows C_L and *L/D* as functions of α for the three vehicles.

Most notable is that the vehicles do not fly at the angles of attack of their respective maximum lift-to-drag ratio's. A decrease in angle of attack (to obtain a higher *L/D*) is not possible, because in that case the lift coefficient decreases, and subsequently (see equation (5)) the heat flux and wall temperature increase.

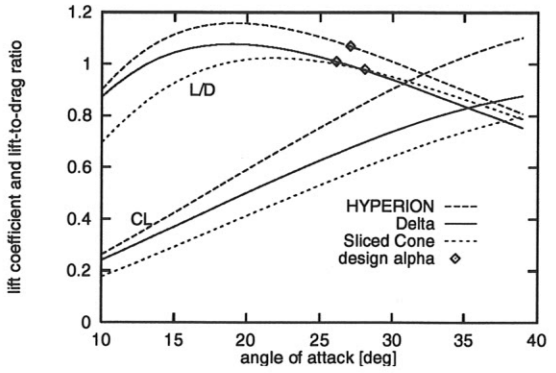

Figure 12: Lift-to-drag ratios and lift coefficients as function of angle of attack for optimal vehicles

Densities are considerably higher than those of Colibri and HYFLEX. Compared to Colibri, the current vehicles have a somewhat higher *L/D* and C_L. At given mass, this allows the nose radius and the reference area to be smaller (see equation (3)), therefore the volume to be smaller, and thus the density to be higher. In comparison to HYFLEX, higher heat fluxes and temperatures are allowed, which also results in a higher density.

The volumetric efficiencies break the trend of figure 3. The ratio of equation (3) for a slender cone-like shape such as HYPERION is comparable to a winged vehicle such as the Space Shuttle. The hypersonic *L/D*'s are comparable as well, and because cross and down range are solely obtained in the hypersonic regime, the performance of both vehicles are comparable. This is also illustrated by the biconic concepts that have been proposed as Hermes replacements. They still gave similar flexibility in cross and down range, but at reduced vehicle complexity. Landing is done using parachutes, whereas the Shuttle uses wings during the final (super- and subsonic) stages of the flight.

Figures 13 and 14 give the possible locations of the centre of mass, such that the vehicle is trimmed and statically stable, for a flap chord of 0.2 m and flap deflections of -5° to 15°. Figure 10 gives the general location for HYPERION, and figure 11 gives a more detailed view of all three areas. All three areas are of similar shape, and are delimited on the forward side by the most forward location of the *c.o.m.* at $\alpha = 45°$ and $\delta = -5°$. The aft-upper boundary is formed by the static stability constraint at $\alpha = 15°$ for flap deflection between -5° and 15°. In effect this boundary is formed by intersections of lines for *c.o.m.* with lines for $C_{M_\alpha} = 0$ for $\delta = -5°$ to 15°. The lower aft boundary is formed by the location of the *c.o.m.* at $\alpha = 15°$ for $\delta = 15°$.

It is clear that the sliced cone has the largest area, which is about 2 to 3 times larger then for HYPERION and Delta. The difference between the sliced cone and HYPERION is primarily in *c.o.m.* travel in x-direction. This is understandable when considering the flap width,

which is about is 50 % larger for the sliced cone than for HYPERION and Delta.

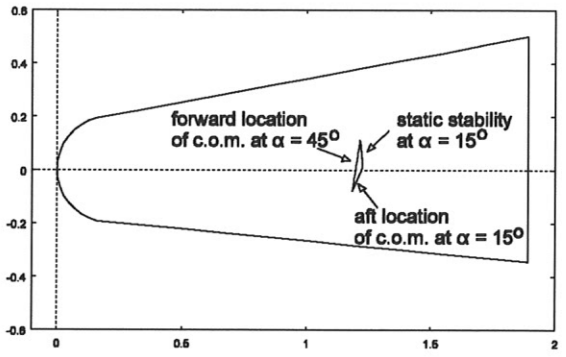

Figure 13: Possible locations of centre of mass of HYPERION

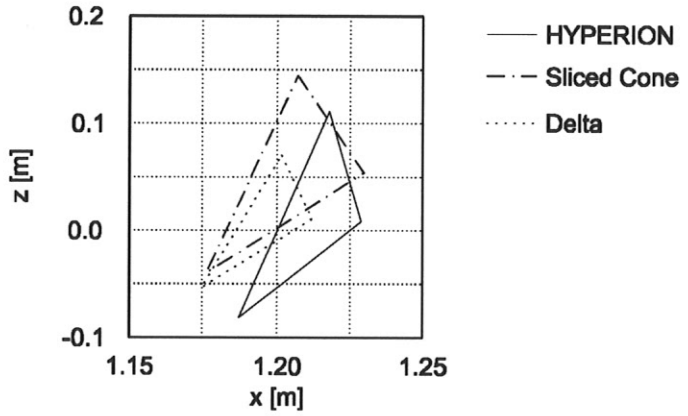

Figure 14: Possible locations of centre of mass of the three shapes

Table 8 shows this result again as the maximum allowable *c.o.m.* travel in x-direction as percentage of body length. An increase of flap chord length to 0.3 m gives a considerable increase in the *c.o.m.* travel of about 70 to 115%. The sliced cone has not only the largest allowable *c.o.m.* travel, but also shows the largest increase in *c.o.m.* travel. An increase in flap chord length could be constrained by the available space. In that case it is also possible to move the hinge axis forward. However, this will result in a somewhat lower moment, due to the reduced distance to the centre of mass.

	c.o.m. travel % of body length	
	c_f = 0.2 m	c_f = 0.3 m
HYPERION	1.4	2.4
Delta	1.3	2.5
Sliced cone	2.0	4.3

Table 8: Maximum *c.o.m.* travel in x-direction

6 Conclusions and recommendations

The refined method as compared to the previous method (1) gives more exact results for aerodynamics, that are favourable for the overall aerodynamic quality, (2) allows optimization of complex vehicles with a great number of variables including flap lengths, flap deflections and centre of mass location, (3) has a more accurate heat flux model that has been identified and implemented, and (4) uses the wall temperature as constraint, which is directly related to construction materials.

The update of HYPERION has a considerable better *L/D*, Partially this is because aerodynamics were estimated using the exact geometry and secondly because the much lower mass allowed a smaller nose radius and thus a better *L/D*.

The lift-to-drag ratios of the three alternatives do not differ considerably, but the sliced cone gives a considerable more generous travel of the centre of mass. An increase in flap chord greatly improves the *c.o.m.* travel. A 50% increase of flap chord about doubles the *c.o.m.* travel. Therefore it could be profitable to change body length to flap chord length, or to shift the hinge axis forward when increasing the flap chord.

Other aspects that did not come forward in this paper and that require further attention are: (1) A more thorough investigation of the heat flux methods, which show a large difference, and have a considerable effect on the final result. (2) The use of the equilibrium glide approximation, which does not take into account the entry at non-equilibrium conditions at large angles of attack. A comparison with a more sophisticated trajectory optimization tool should be made to check this approximation.

For a proper selection of one of the shapes further attention is required for directional stability, in particular at high angles of attack, weight estimation and TPS design, flow phenomena and structural layout.

References

Anderson, J.D. Jr.
Hypersonic and High Temperature Gas Dynamics
McGraw-Hill, 1989

Bannink, W.J.
Lecture notes: Introduction to Hypersonic Aerodynamics
in Dutch, Delft University of Technology, Faculty of Aerospace Engineering, April 1994

Cazaux, Ch., Pardessus, Th. and Breard G.
The Atmospheric Re-entry Demonstrator
Deutscher Luft- un Raumfahrt-Kongress, 1995

Chapman, D.R.
An approximate analytical method for studying entry into planetary atmospheres
NASA TR-R-11, Ames Research Centre, CA, 1959

Curry, D.M. and Rochelle, W.C., Chao, D.C. and Ting, P.C.
Space Shuttle Orbiter Nose Cap Thermal Analysis
AIAA-86-0388, January 1986

Griffin, M.D. and French, J.R.
Space Vehicle Design
AIAA Education Series, 1991

Harris, T.B., Wall D.W. and Martelli, A.
Aerodynamic Prediction Methodology for Manoeuvring Re-entry Vehicles
AIAA Atmospheric Flight Mechanics Conference, AIAA-80-1609, August 1980

Huizinga, M.
HYPERION, Experimental Re-entry Investigation Of the Netherlands
AX-96.066, NLR, National Aerospace Laboratory, November 1996

IMSL
User's Manual, Math/Library, FORTRAN Subroutines for Mathematical Applications, Version 1.0
IMSL, April 1987

Jane's All The World's Aircraft, 1964

Jane's All The World's Aircraft, 1969

Kemp, N.H. and Ridell, F.R.
Heat transfer to Satellite Vehicles Reentering the Atmosphere
Jet Propulsion, 1957, pp 132-147

Koppenwallner, G.
Aerothermodynamik- Ein Schlüssel zu neuen Transportgeräten der Luft- und Raumfahrt
Zeitschrift für Flugwissenschaften und Weltraumforschung, Vol. 12, 1988, pp 6-18

Mooij, E., Marée, A.G.M. and Sudmeijer, K.J.
Aerodynamic Controllability of a Selected Re-entry Test Vehicle
IAF-95-V.4.04, October 1995

MPSO
Alternate Carriers for Experiments
Microgravity Program Support Office, July 1995

Romagnoli, L.
Preliminary Design of HYPERION: Re-entry Test Vehicle, Design Method Formulation and Verification
Master Thesis, University of Pisa, Faculty of Aerospace Engineering, July 1996

Schöttle, U.M. and Burkhardt, J.
Entwurf einer kleinen semibalistischen Rückkehrkapsel
Space Course Stuttgart, 1995

Shirouzu, M. and Watanabe, S.
On the Hypersonic Flight Experiment (HYFLEX) for the Development of HOPE
AIAA-93-5080, December 1993

Stewart, J.D. and Greenshields, D.H.
Entry Vehicles for Programs
Journal of Spacecraft and Rockets, Vol. 6, Nr. 10, pp 1089-1102, October 1969

Sudmeijer, K.J. and Hagmeijer, R.
LARVE, a hypersonic flight-test facility launched by Ariane-4
Workshop Proceedings, Flight Opportunities for Small Payloads, ESA SP-298, February 1989

Sudmeijer, K.J.
Aerodynamic design and Centre of Gravity of the HYPERION re-entry module
FS/LA-R-96-0008, Fokker Space, May 1996

Tauber, M.E., Menees, G.P. and Adelman, H.G.
Aerothermodynamics of Transatmospheric Vehicles
AIAA-86-1257, June 1986

Teutsch, J and Zandbergen, B.T.C.
Design Update of the Aerodynamically Controlled Re-entry Test Vehicle HYPERION using a Refined Method
DUT-FAE, To Be Published

Veldman, S.M.
Program for Estimation of Aerodynamic Characteristics of Hypersonic vehicles: PEACH; program formulation and verification
Master Thesis, Delft University of Technology, Faculty of Aerospace Engineering, July 1994

Veldman, S.M. and Zandbergen, B.T.C.
Spaceplane Aeroheating: Some Simple Estimation Methods
Delft University of Technology, Faculty of Aerospace Engineering, To Be Published

Vinh, N.X., Busemann, A. and Culp, R.D.
Hypersonic and planetary entry flight mechanics
The University of Michigan Press, Ann Arbor, 1980

Williams, S.D. and Curry, D.M.
Assessing the Orbiter Thermal Environment Using Flight Data
Journal of Spacecraft and Rockets, Vol. 21, No. 6, pp 534-541, 1984